



Cite this: *Catal. Sci. Technol.*, 2015, 5, 3288

# Synthesis of novel MgAl layered double oxide grafted TiO<sub>2</sub> cuboids and their photocatalytic activity on CO<sub>2</sub> reduction with water vapor†

Cunyu Zhao,<sup>a</sup> Lianjun Liu,<sup>a</sup> Guiying Rao,<sup>a</sup> Huilei Zhao,<sup>b</sup> Luhui Wang,<sup>c</sup> Jinye Xu<sup>a</sup> and Ying Li<sup>\*b</sup>

A series of magnesium/aluminum (MgAl) layered double oxide (LDO) grafted TiO<sub>2</sub> cuboids (MgAl-LDO/TiO<sub>2</sub>) with various molar ratios of (Mg + Al) to Ti were synthesized by a combination of hydrothermal and coprecipitation methods, in which the growth of MgAl-LDO platelets was controlled. The MgAl-LDO/TiO<sub>2</sub> composite materials were used for photocatalytic CO<sub>2</sub> reduction with water vapor under UV light irradiation in a continuous-flow reactor. CO was found to be the main product from CO<sub>2</sub>. At near room temperature (e.g., 50 °C), MgAl-LDO/TiO<sub>2</sub> did not significantly enhance CO<sub>2</sub> reduction compared with pure TiO<sub>2</sub> cuboids. At a moderately elevated reaction temperature (e.g., 150 °C), the MgAl-LDO/TiO<sub>2</sub> sample with an optimum 10 wt.% MgAl-LDO loading demonstrated CO<sub>2</sub> reduction activity five times higher than that of bare TiO<sub>2</sub> cuboids. The photo-induced electrons on TiO<sub>2</sub> may migrate to the MgAl-LDO/TiO<sub>2</sub> interfacial sites to promote CO<sub>2</sub> reduction. Findings in this work may lead to a new area of hybrid adsorbent/photocatalyst materials that are capable of sequential CO<sub>2</sub> capture and photocatalytic conversion.

Received 9th February 2015,  
Accepted 6th April 2015

DOI: 10.1039/c5cy00216h

www.rsc.org/catalysis

## 1. Introduction

Emission of carbon dioxide (CO<sub>2</sub>) from consumption of fossil fuels is one of the main causes of global climate change. Photocatalytic reduction of CO<sub>2</sub> with water under sunlight has been considered as a promising way to lower the CO<sub>2</sub> level in the atmosphere, meanwhile producing alternative fuels such as carbon monoxide (CO), methane (CH<sub>4</sub>) and methanol.<sup>1,2</sup> Among the various photocatalyst materials, TiO<sub>2</sub> is widely studied due to its suitable band positions, environmentally benign nature, low cost and easy availability.<sup>3–6</sup> However, photocatalytic CO<sub>2</sub> reduction with water using TiO<sub>2</sub> as the photocatalyst typically has low energy conversion efficiency.<sup>1,2,7,8</sup> This is because of the major obstacles including the fast recombination rate of photo-generated electron-hole (e–h) pairs, the wide band gap of TiO<sub>2</sub> (3.2 eV for anatase), and the fast backward reactions.<sup>5,9</sup> Approaches such as loading noble metal or metal oxides and doping with non-metal elements have been applied to improve the CO<sub>2</sub>

photoreduction activity of TiO<sub>2</sub>.<sup>1,10,11</sup> In addition to these well-known challenges, there are other factors that hinder the photocatalytic activity but are rarely studied in the literature, such as the weakened CO<sub>2</sub> adsorption on TiO<sub>2</sub> at the solid–gas interface in the presence of water vapor and limited desorption of reaction products or intermediates from the catalyst surface.<sup>12,13</sup> As a result, enhancing the CO<sub>2</sub> adsorption on the photocatalyst, a prior step to photoreduction, is important to improve the CO<sub>2</sub> photoreduction efficiency of hydrocarbon fuels.

Our previous studies have reported MgO–TiO<sub>2</sub> composites as hybrid adsorbent/photocatalyst materials for enhanced CO<sub>2</sub> photoreduction.<sup>12,13</sup> MgO was chosen as the CO<sub>2</sub> adsorbent because of its good CO<sub>2</sub> adsorption capability that is boosted in the presence of H<sub>2</sub>O vapor.<sup>14–16</sup> We found that MgO–TiO<sub>2</sub> possessed much higher activity and more stable performance than pristine TiO<sub>2</sub>, particularly at a medium temperature range (around 150 °C), which may be due to the easier desorption of reaction intermediates at a higher temperature and the enhanced CO<sub>2</sub> adsorption by MgO compared with bare TiO<sub>2</sub>. We also reported that the concentration and dispersion of MgO on the MgO/TiO<sub>2</sub> composite strongly influenced the CO<sub>2</sub> photoreduction activity and 5% MgO was the optimum loading on the TiO<sub>2</sub> surface. However, since both MgO and TiO<sub>2</sub> were in the form of nanoparticles in the MgO/TiO<sub>2</sub> composites, it was difficult to distinguish the two components by microscopic analysis and to correlate the catalytic activity with the materials morphology or

<sup>a</sup> University of Wisconsin–Milwaukee, Mechanical Engineering Department, Milwaukee, WI 53211, USA

<sup>b</sup> Texas A&M University, Department of Mechanical Engineering, College Station, TX 77843, USA. E-mail: yingli@tamu.edu; Fax: +1 979 845 3081; Tel: +1 979 862 4465

<sup>c</sup> Zhejiang Ocean University, Chemical Engineering Department, Zhejiang, PR China

† Electronic supplementary information (ESI) available. See DOI: 10.1039/c5cy00216h

structure. In addition, MgO has been reported to have relatively low kinetics in CO<sub>2</sub> adsorption at moderate temperatures (250–400 °C) possibly due to the changing of basic sites or –OH groups.<sup>17,18</sup> Hence, other medium temperature CO<sub>2</sub> sorbents with different morphologies and faster adsorption kinetics may be of greater interest to serve as the adsorbent component of the hybrid material for enhanced CO<sub>2</sub> photoreduction.

Layered double hydroxides (LDHs), also known as hydrotalcite-like compounds, and their post-calcination product, layered double oxides (LDOs), have been investigated as CO<sub>2</sub> sorbents.<sup>19–21</sup> LDHs can be chemically expressed by general formula  $M_{1-x}^{2+}M_x^{3+}(\text{OH})_2A_x \cdot n\text{H}_2\text{O}$ , where  $M^{2+}$  and  $M^{3+}$  are metal ions and A stands for exchangeable anions ( $\text{Cl}^-$ ,  $\text{NO}_3^-$ ,  $\text{CO}_3^{2-}$ , or  $\text{SO}_4^{2-}$ ).<sup>22–25</sup> The characteristics of LDHs provide the LDO properties with a large number of Brønsted basic sites, and thus LDOs are considered as promising candidates for CO<sub>2</sub> adsorption,<sup>26</sup> and activated MgAl-LDOs are found to have a high sorption capacity for CO<sub>2</sub>.<sup>19,21,27</sup> It is reported that MgAl-LDOs can capture much more CO<sub>2</sub> than MgO at the medium temperature range 150–450 °C.<sup>28,29</sup> Hence, MgAl-LDO could be a good candidate as a replacement of MgO to combine with the TiO<sub>2</sub> photocatalyst to improve CO<sub>2</sub> photoreduction operated at a medium temperature (~150 °C).

The objective of this work is to design a novel hybrid adsorbent/photocatalyst material by grafting MgAl-LDOs (as the CO<sub>2</sub> adsorbent component) onto the surface of micrometer size TiO<sub>2</sub> cuboids (as the photocatalyst component) and to investigate the catalytic activity of CO<sub>2</sub> photoreduction in correlation with the materials properties. To obtain such a hybrid material structure, it is desirable to have micrometer size TiO<sub>2</sub> for MgAl-LDO grafting because MgAl-LDOs are reported to be micrometer or sub-micrometer size platelets. The platelet-shape MgAl-LDOs can be distinct from the micrometer-size TiO<sub>2</sub> cuboids, and thus, the morphology and concentration of the two components can be easily manipulated.

## 2. Experimental

### 2.1. Synthesis of MgAl-LDO grafted TiO<sub>2</sub> cuboids

The MgAl-LDH grafted TiO<sub>2</sub> cuboids were synthesized by a two-step process that has not been reported before. In the first step hydrogenated titanate (H<sub>2</sub>Ti<sub>3</sub>O<sub>7</sub>) nanobelts were produced and in the second step, MgAl-LDH was formed by coprecipitation with the H<sub>2</sub>Ti<sub>3</sub>O<sub>7</sub> nanobelts that were transformed into a cuboid shape along the coprecipitation process. H<sub>2</sub>Ti<sub>3</sub>O<sub>7</sub> nanobelts (micrometers in length) were prepared *via* a hydrothermal method that has been widely reported in the literature.<sup>30–32</sup> Typically, 1.0 g of TiO<sub>2</sub> (Aeroxide P90) was dispersed in 60 ml of 10 M NaOH aqueous solution with a 1:1 H<sub>2</sub>O/ethanol volume ratio. The solution was kept stirring for 30 min and then transferred to a Teflon-lined autoclave. The sodium titanate obtained after 16 h of hydrothermal conditions at 180 °C was washed with 0.1

M HCl aqueous solution until pH 3–4 and then washed with deionized (DI) water until pH 7, forming H<sub>2</sub>Ti<sub>3</sub>O<sub>7</sub> nanobelts.

In the second step, the MgAl-LDH grafted TiO<sub>2</sub> cuboids were prepared by a coprecipitation method. The as-prepared H<sub>2</sub>Ti<sub>3</sub>O<sub>7</sub> nanobelts were re-dispersed in 30 ml of 3.0 M urea solution to form solution A. Mg(NO<sub>3</sub>)<sub>2</sub>·6H<sub>2</sub>O and Al(NO<sub>3</sub>)<sub>3</sub>·9H<sub>2</sub>O were dissolved in 30 ml of DI water with  $[\text{Mg}^{2+}] + [\text{Al}^{3+}] = 0.15 \text{ M}$ ,  $n(\text{Mg})/n(\text{Al}) = 2:1$  to obtain solution B. Solution B was dropwise added into solution A under stirring. The mixture was transferred to a round bottom flask in an oil bath. The flask was equipped with a water condenser with cooling water. The temperature for the mixture was set to be ~95 °C and was kept under continuous magnetic stirring for 12 h. The obtained precipitate was washed with DI water until pH 7 and vacuum dried at 80 °C overnight to form MgAl-LDH grafted TiO<sub>2</sub>. Finally, the powder was calcined at 400 °C for 3 hours to form MgAl-LDO grafted TiO<sub>2</sub>. To find the optimum MgAl-LDO concentration in the composites to obtain the best photocatalytic CO<sub>2</sub> reduction activity, the samples with different mass ratios of MgAl-LDO to TiO<sub>2</sub> were prepared. The samples were denoted as x% MgAl-LDO/TiO<sub>2</sub>, in which x represents the measured weight percentage of MgAl-LDO in the sample. Pure TiO<sub>2</sub> cuboids were also synthesized as the control.

### 2.2. Materials characterization

The crystal structures of the MgAl-LDO/TiO<sub>2</sub> samples were identified by X-ray diffraction (XRD, Scintag XDS 2000) using Cu K $\alpha$  irradiation at 45 kV and a diffracted beam monochromator at 40 mA. The optical properties were examined by UV-vis diffuse reflectance spectroscopy using a UV-vis spectrometer (Ocean Optics) with BaSO<sub>4</sub> as the background. Scanning electron microscopy (SEM) (Hitachi S4800) was used to investigate the catalyst morphology. The dispersion of elements (Mg, Al, Ti, O) on MgAl-LDO/TiO<sub>2</sub> was analyzed by X-ray elemental mapping. The real concentration of MgAl-LDO in the sample was calculated by the difference of the weight of MgAl-LDO/TiO<sub>2</sub> before and after washing and drying with 1 M HCl solution.

The Brunauer–Emmett–Teller (BET) specific surface area of the composites was measured by nitrogen adsorption at 77 K on a surface area and porosity analyzer (Micrometrics ASAP 2020). Before each adsorption measurement, approximately 0.10 g of the sample was degassed at 180 °C for 6 hours. The BET surface area was determined by a multipoint BET method using the adsorption data in the relative pressure ( $P/P_0$ ) range 0.05–0.3. The thermal stability of the catalyst materials was carried out using a thermogravimetric analyzer (TGA-DAT-2960 SDT) at a heating rate of 20 °C min<sup>−1</sup> from 25 to 700 °C in air.

### 2.3. Measurement of CO<sub>2</sub> photoreduction activity

The photocatalytic reduction of CO<sub>2</sub> with H<sub>2</sub>O vapor was conducted using a home-made quartz tube photoreactor operating in a continuous flow mode, as shown in Fig. S1.†



For each test, 100 mg of the catalyst was used and evenly dispersed onto a rectangular glass-fiber filter that was placed alongside the wall of the quartz tube and facing the UV light illumination. The catalyst loading process is also shown in Fig. S1.† CO<sub>2</sub> cylinder gas (99.999%, Praxair) continuously passed through a DI water bubbler bringing a gas mixture of CO<sub>2</sub> + H<sub>2</sub>O (with 2.3 vol.% H<sub>2</sub>O) into the photoreactor. A high gas flow rate was used initially to purge out air inside the reactor for 2 h, which in the meantime ensured CO<sub>2</sub> adsorption reaching equilibrium on the catalyst surface. Then the flow rate was lowered and maintained at 2.0 sccm during photoreaction. A 100 W mercury vapor lamp or a 450 W Xe lamp with a 400 nm UV cut-off filter was used as the UV-vis light and visible light source, respectively, and the light spectra are shown in Fig. S2.† For the mercury vapor lamp, the light intensity was measured to be about 10 mW cm<sup>-2</sup> in the UV region ( $\lambda < 390$  nm, centered at 365 nm). As a reference, the UV intensity in the sunlight (AM1.5G) is around 5 mW cm<sup>-2</sup>. Thus, the UV intensity from the mercury vapor lamp applied in this study was equivalent to approximately 2 suns. For the Xe lamp with a UV filter, the light intensity in the visible region (400–700 nm) was about 84 mW cm<sup>-2</sup>, again close to 2-sun conditions. To reach and maintain a reaction temperature at 150 °C, the optimum temperature found in our previous work for MgO–TiO<sub>2</sub> catalysts,<sup>13</sup> a 250 W infrared lamp was used to heat up the photoreactor and the temperature can be adjusted by varying the distance between the IR lamp and the reactor. The gaseous products in the reactor effluent were continuously analyzed at a 15 min interval using a gas chromatograph (GC, Agilent 7890A) equipped with an automated gas valve and a thermal conductivity detector (TCD) and flame ionization detector (FID).

### 3. Results and discussion

#### 3.1. Crystal structure of MgAl-LDO/TiO<sub>2</sub>

Fig. 1 shows the XRD patterns for MgAl-LDH, MgAl-LDO, 10% MgAl-LDH/TiO<sub>2</sub>, 10% MgAl-LDO/TiO<sub>2</sub> and TiO<sub>2</sub> cuboid samples. The diffraction peaks in both MgAl-LDH and 10% MgAl-LDH/TiO<sub>2</sub> patterns were indexed to MgAl-LDH<sup>19,23,33</sup> and weaker peaks were observed for the 10% MgAl-LDH/TiO<sub>2</sub> sample compared with MgAl-LDH. No TiO<sub>2</sub> characteristic peaks were observed for 10% MgAl-LDH/TiO<sub>2</sub> indicating that the TiO<sub>2</sub> crystal phase was not formed without calcination. For TiO<sub>2</sub> cuboids, all the diffraction peaks were attributed to the anatase phase [JCPDS no. 21-1272].<sup>2,7,8</sup> For the MgAl-LDO sample, all the diffraction peaks were indexed to MgO.<sup>12,19,34</sup> For the 10% MgAl-LDO/TiO<sub>2</sub> samples, only TiO<sub>2</sub> anatase diffraction peaks are observed, and no MgO diffraction peaks are seen. The Scherrer equation was applied to calculate the crystallite size of TiO<sub>2</sub>. The diffraction peaks of TiO<sub>2</sub> anatase in 10% MgAl-LDO/TiO<sub>2</sub> composites are narrow compared with TiO<sub>2</sub> cuboids, suggesting a larger crystallite size of TiO<sub>2</sub> due to MgAl-LDO addition. The average crystallite size of TiO<sub>2</sub> anatase in TiO<sub>2</sub> cuboids was 15 nm. By comparison, the average crystallite size of TiO<sub>2</sub> anatase in 10% MgAl-LDO/

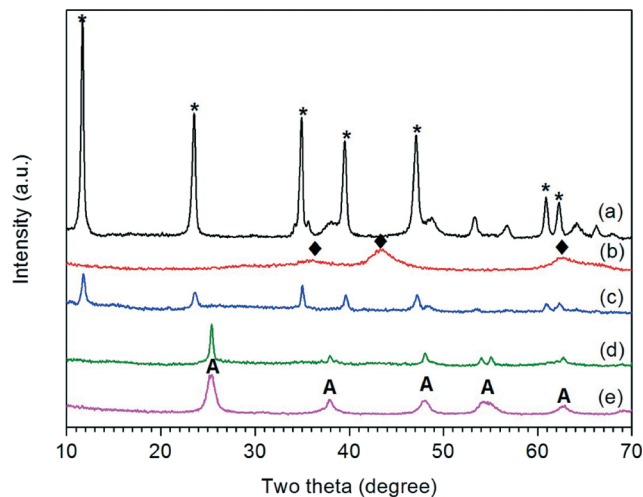


Fig. 1 XRD patterns of samples: (a) MgAl-LDH; (b) MgAl-LDO; (c) 10% MgAl-LDH/TiO<sub>2</sub>; (d) 10% MgAl-LDO/TiO<sub>2</sub> and (e) TiO<sub>2</sub> cuboids (\* represents MgAl-LDH characteristic peaks, A represents TiO<sub>2</sub> anatase, and ◆ represents MgO characteristic peaks).

TiO<sub>2</sub> composites was 32 nm. A possible reason is that the addition of Mg(NO<sub>3</sub>)<sub>2</sub> and Al(NO<sub>3</sub>)<sub>3</sub> consumes urea during the second step of materials synthesis and helps preserve some of the H<sub>2</sub>Ti<sub>3</sub>O<sub>7</sub> nanobelts that are later transformed to crystalline TiO<sub>2</sub> anatase.<sup>32</sup>

#### 3.2. Morphology, textural structure and optical property of MgAl-LDO/TiO<sub>2</sub>

Fig. 2 shows the SEM images of H<sub>2</sub>Ti<sub>3</sub>O<sub>7</sub> titanate nanowires (precursor to TiO<sub>2</sub> cuboids), MgAl-LDOs and TiO<sub>2</sub> cuboids. MgAl-LDOs consist of platelets around 2 μm in size. The length of the TiO<sub>2</sub> cuboids is in the micrometer size range with a high aspect ratio. The length of TiO<sub>2</sub> cuboids pretty much agrees with that of the titanate nanowires, suggesting that the cuboids are indeed transformed from nanowires during the second step of materials synthesis.

The textural properties are characterized by BET analysis and the results are summarized in Table 1. Bare TiO<sub>2</sub> cuboids displayed a specific surface area of 109 m<sup>2</sup> g<sup>-1</sup> and a pore volume of 0.48 cm<sup>3</sup> g<sup>-1</sup>, where the pores are probably attributed to inter-nanoparticle spacing. The MgAl-LDO had a specific surface area of 180 m<sup>2</sup> g<sup>-1</sup>, greater than that of TiO<sub>2</sub> cuboids, possibly due to the smaller interplanar spacing between the layered oxides, which is also reflected by the smaller pore size. Notably, the 10% MgAl-LDO/TiO<sub>2</sub> sample possessed a high specific surface area (175 m<sup>2</sup> g<sup>-1</sup>) close to the bare MgAl-LDO, although the concentration of MgAl-LDO was not high. This indicates certain interaction between the MgAl-LDH nanoflakes and TiO<sub>2</sub> nanoparticles during the formation of the hybrid material.

The thermogravimetric analysis (TGA) result of the 10% MgAl-LDH/TiO<sub>2</sub> sample is given in Fig. S3,† which shows two main steps of weight loss which are consistent with the literature.<sup>22</sup> The adsorbed water in LDH was released at a relatively





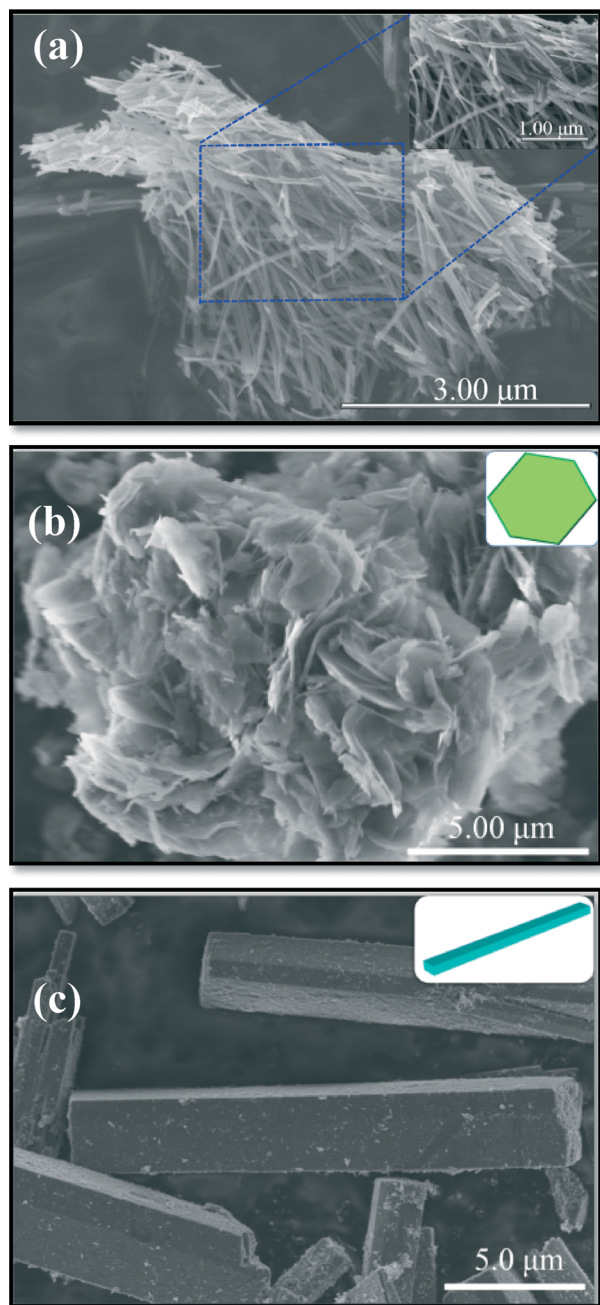


Fig. 2 SEM images of (a)  $\text{H}_2\text{Ti}_3\text{O}_7$  titanates, (b) MgAl-LDOs and (c)  $\text{TiO}_2$  cuboids.

low temperature to 200 °C where it was mostly in the form of interlamellar water. Carbonate ions of the LDH sample were decomposed at higher temperatures from 200 to 500 °C in parallel with the water loss. The weight loss almost ceased at

above 500 °C indicating the completion of the decarbonation process, *i.e.*, LDH was fully converted to LDO.

Fig. 3 shows the SEM images of MgAl-LDO/ $\text{TiO}_2$  samples with different compositions. The lower magnification SEM images in Fig. 3a, c, and e show that the three samples were composed of MgAl-LDOs grafted on micrometer size  $\text{TiO}_2$  cuboids. The platelet shape of MgAl-LDOs on the composites after calcination was almost the same as the as-prepared uncalcined composites MgAl-LDHs (SEM images not shown here). In most of the literature reports, the morphology of MgAl-LDH platelets cannot be maintained after calcination.<sup>25,35</sup> The successful grafting of MgAl-LDO platelets on micrometer-size  $\text{TiO}_2$  cuboids in this work demonstrates a novel approach in synthesizing such composite materials with the desired morphology. The higher magnification SEM images in Fig. 3b, d, and f show that both the size and the coverage of MgAl-LDO platelets grafted on  $\text{TiO}_2$  cuboids increased as the MgAl-LDO loading increased.

The distributions of Mg, Al, Ti and O elements in the MgAl-LDO/ $\text{TiO}_2$  composites were analyzed by X-ray elemental mapping, and the results are shown in Fig. 4. The elemental mapping images demonstrated that the cuboid skeletons were mainly composed of the Ti element and the grafted platelets were composed of Mg and Al elements that were evenly distributed on the cuboid surface. The O element is distributed on both the cuboids and the platelets, agreeing with the composition of mixed oxides for this composite material.

Diffuse reflectance UV-vis spectra were recorded to investigate the influence of MgAl-LDO on the optical property of  $\text{TiO}_2$ , and the plots of Kubelka–Munk function were made to determine the band gap values, as shown in Fig. 5. The absorption edge of the  $\text{TiO}_2$  is around 390 nm, corresponding to a band gap of about 3.2 eV, which agrees with most reported literature data on the band gap of  $\text{TiO}_2$  anatase. The MgAl-LDO alone shows no light adsorption in the wavelength range measured. The incorporation of MgAl-LDOs on  $\text{TiO}_2$  cuboids leads to a slight blue-shift in the adsorption edge and a reduced absorption in the UV region, probably due to the increased surface roughness resulting in more reflection.

To further confirm possible structural changes, UV/Vis adsorption spectra of  $\text{H}_2\text{Ti}_3\text{O}_7$  and 10% MgAl-LDH/ $\text{TiO}_2$  were recorded as shown in Fig. S4.† By comparing  $\text{TiO}_2$  cuboids with  $\text{H}_2\text{Ti}_3\text{O}_7$ , it is observed that  $\text{TiO}_2$  cuboids have a red-shift in the absorption edge, which indicates compositional changes due to the calcination of  $\text{H}_2\text{Ti}_3\text{O}_7$ . By comparing 10% MgAl-LDH/ $\text{TiO}_2$  with 10% MgAl-LDO/ $\text{TiO}_2$ , difference in the absorption shift is also observed due to the conversion of LDH to LDO. By comparing MgAl-LDO/ $\text{TiO}_2$  with  $\text{TiO}_2$

Table 1 Textural properties of  $\text{TiO}_2$ , MgAl-LDO and MgAl-LDO/ $\text{TiO}_2$  samples

Sample	BET specific surface area ( $\text{m}^2 \text{g}^{-1}$ )	Pore volume ( $\text{cm}^3 \text{g}^{-1}$ )	Pore size (nm)
$\text{TiO}_2$ cuboids	109	0.48	16
10% MgAl-LDO/ $\text{TiO}_2$	175	0.39	9
MgAl-LDO	180	0.28	8



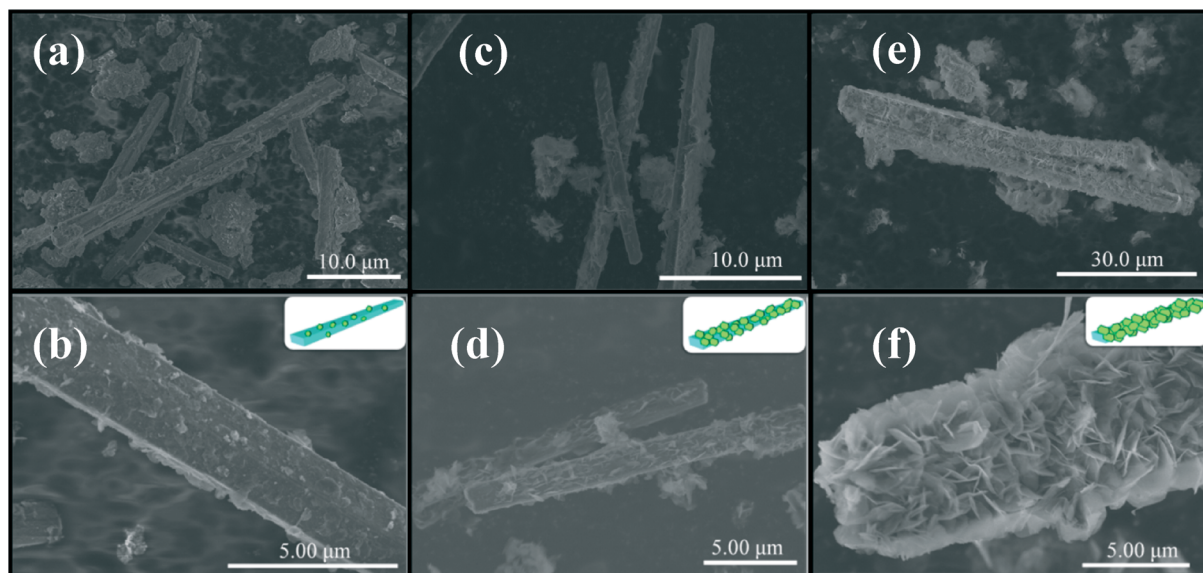


Fig. 3 SEM images of the MgAl-LDO/TiO<sub>2</sub> composites: (a, b) 8% MgAl-LDO/TiO<sub>2</sub>, (c, d) 10% MgAl-LDO/TiO<sub>2</sub>, and (e, f) 12% MgAl-LDO/TiO<sub>2</sub>.

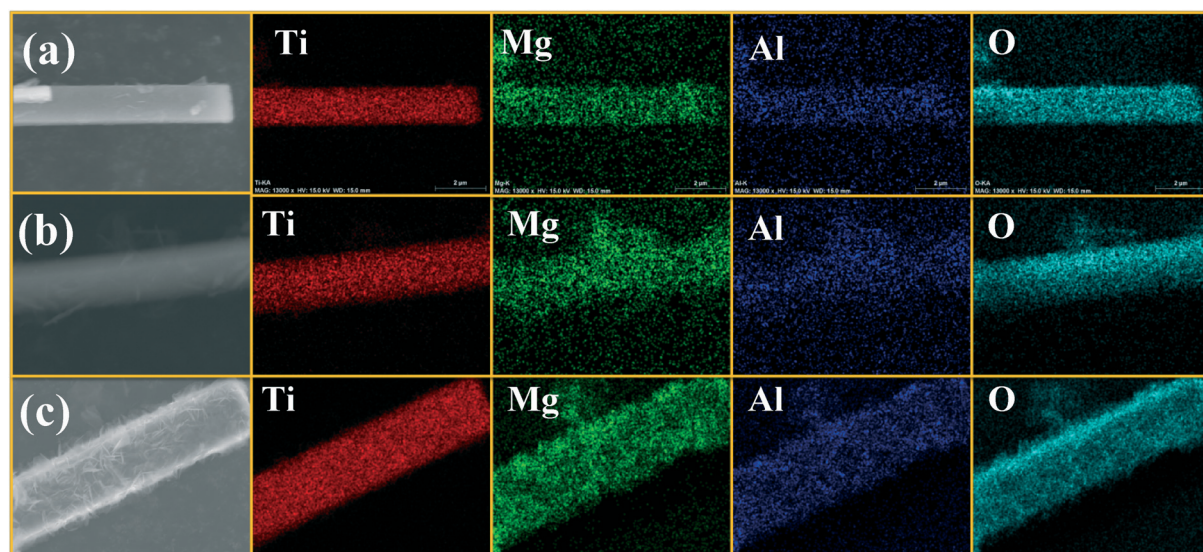


Fig. 4 X-ray elemental mapping images of the MgAl-LDO/TiO<sub>2</sub> composites: (a) 8% MgAl-LDO/TiO<sub>2</sub>, (b) 10% MgAl-LDO/TiO<sub>2</sub>, and (c) 12% MgAl-LDO/TiO<sub>2</sub>.

cuboids, it is observed that there is less absorption in the UV region for the MgAl-LDO/TiO<sub>2</sub>, which indicates possible interaction of MgAl-LDO with TiO<sub>2</sub>.<sup>36</sup> From the XRD results, there is no obvious change of TiO<sub>2</sub> diffraction peaks or appearance of new peaks, suggesting that the extent of Mg atom incorporation into the TiO<sub>2</sub> structure, if any, is not significant.

### 3.3. Photocatalytic activities of CO<sub>2</sub> reduction

Photocatalytic activity tests were carried out under UV light irradiation at 50 °C for 4 h (Fig. 6a) and subsequently at 150 °C for another 8 h (Fig. 6b). CO was found to be the major product with a minor CH<sub>4</sub> concentration that was one or two orders of magnitude lower than CO. Thus, only CO production results were shown in Fig. 6 to compare the activities of

the different catalysts. Fig. 6a shows that bare TiO<sub>2</sub> cuboids had a CO production rate of around 1.0 μmol g<sup>-1</sup> h<sup>-1</sup> at 50 °C while pure MgAl-LDO had no activity for CO production. The addition of MgAl-LDO on TiO<sub>2</sub> cuboids had no significant improvement in the CO production rate except for the 10% MgAl-LDO/TiO<sub>2</sub> sample that has a doubled activity compared with bare TiO<sub>2</sub> cuboids. The main reason for such insignificant improvement is maybe because MgAl-LDOs has weak CO<sub>2</sub> adsorption at low temperatures.<sup>26</sup>

For the following 8 h test under UV light at 150 °C (Fig. 6b), the CO production rate of bare TiO<sub>2</sub> cuboids was almost the same as the first 4 hours at 50 °C. Pure MgAl-LDOs still showed no activity of CO<sub>2</sub> reduction. Both 8% MgAl-LDO/TiO<sub>2</sub> and 10% MgAl-LDO/TiO<sub>2</sub> exhibited an obvious





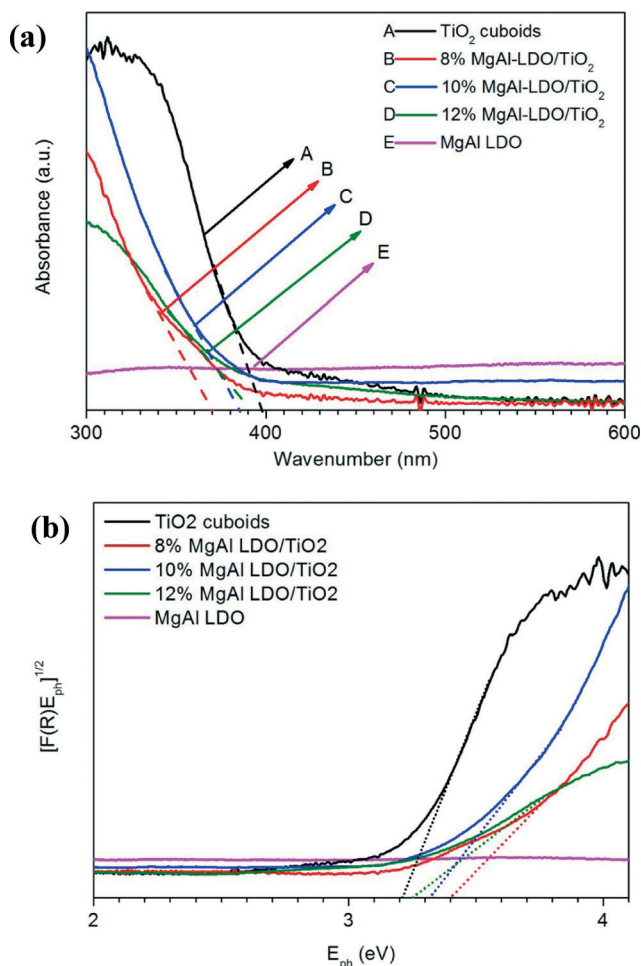


**Fig. 5** (a) UV-vis diffuse reflectance spectra and (b) plots of the square root of Kubelka-Munk function versus the photon energy for the catalyst materials of TiO<sub>2</sub> cuboids, MgAl-LDO, and MgAl-LDO/TiO<sub>2</sub> composites with different MgAl-LDO concentrations.

enhancement in CO production, reaching an average of about 2.8 and 4.3  $\mu\text{mol g}^{-1} \text{h}^{-1}$ , respectively, compared with about 0.7  $\mu\text{mol g}^{-1} \text{h}^{-1}$  for bare TiO<sub>2</sub> cuboids at 150 °C. In other words, 10% MgAl-LDO/TiO<sub>2</sub> was five times more active than bare TiO<sub>2</sub> cuboids. Moreover, the activities of both 8% MgAl-LDO/TiO<sub>2</sub> and 10% MgAl-LDO/TiO<sub>2</sub> at 150 °C were much higher than those at 50 °C. In addition, the downward trend in the CO production rate for the 8% MgAl-LDO/TiO<sub>2</sub> sample indicates that it is inferior to the 10% MgAl-LDO/TiO<sub>2</sub> sample in terms of stability. Interestingly, the activity of 12% MgAl-LDO/TiO<sub>2</sub> did not show any enhancement compared with bare TiO<sub>2</sub> even at 50 °C or 150 °C. The above results indicate that at an optimum MgAl-LDO loading (10% in this study), the CO<sub>2</sub> reduction activity can be significantly increased at a higher temperature (150 °C). It also agrees with our hypothesis that the CO<sub>2</sub> adsorption capability of MgAl-LDOs could promote the CO<sub>2</sub> photoreduction capability by TiO<sub>2</sub>. It is likely that the photo-induced electrons on TiO<sub>2</sub> could migrate to the adjacent CO<sub>2</sub> adsorption sites at the interface of TiO<sub>2</sub> and MgAl-LDO and thus promote CO<sub>2</sub>

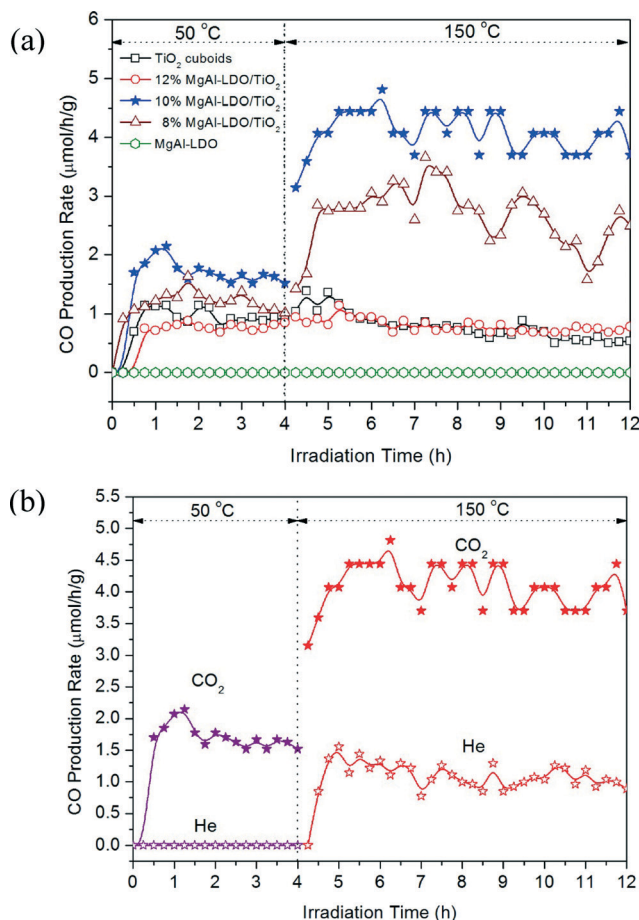


**Fig. 6** The rate of CO production from CO<sub>2</sub> photoreduction under UV light irradiation at 50 °C for 4 h and subsequently at 150 °C for 8 h using (a) TiO<sub>2</sub> cuboids, MgAl-LDO and three MgAl-LDO/TiO<sub>2</sub> composites in the CO<sub>2</sub> + H<sub>2</sub>O vapor atmosphere, and (b) 10% MgAl-LDO/TiO<sub>2</sub> in the He + H<sub>2</sub>O vapor atmosphere and CO<sub>2</sub> + H<sub>2</sub>O vapor atmosphere, respectively.

reduction. However, the exact mechanism is not clear so far and will be investigated in our future research. A very high loading of MgAl-LDO (12% in this case) did not promote CO<sub>2</sub> photoreduction or may have detrimental effect, probably because of the following two reasons: (1) the MgAl-LDOs may have covered all the TiO<sub>2</sub> cuboid surfaces (Fig. 3f) so that the contact between TiO<sub>2</sub> and adsorbed CO<sub>2</sub> is limited, and (2) the light absorption capacity is significantly reduced at a high MgAl-LDO loading (Fig. 5).

The CO<sub>2</sub> photoreduction with H<sub>2</sub>O by the 10% MgAl-LDO/TiO<sub>2</sub> sample under visible light was also carried out using a Xe lamp equipped with a 400 nm cut-off filter, and the result is shown in Fig. S5.† At 50 °C under visible light, the catalyst exhibited no activity and at 150 °C, the CO production rate reached around 1.0  $\mu\text{mol g}^{-1} \text{h}^{-1}$ . Apparently, the material is more active under UV than under visible light, which agrees with the band gap of the material as shown in Fig. 5.

To examine the cycling capability of the catalyst, an additional experiment was conducted using 10% MgAl-LDO/TiO<sub>2</sub> under the mercury vapor lamp irradiation at 150 °C for two



on-and-off cycles for a total period of 12 h. The results are shown in Fig. S6.† The CO production rate was around  $4.0 \mu\text{mol g}^{-1} \text{h}^{-1}$  when light was on. When the light was switched off, the CO production rate decreased rapidly and became zero within one hour. Turning the light back on obviously re-activated the photoreduction and the CO production rate bounced back to  $3.6 \mu\text{mol g}^{-1} \text{h}^{-1}$ , almost the same level as in the first cycle. Switching off the light again led to a stop in the photoreduction. This on-and-off cycling test result clearly indicates that CO production was indeed from  $\text{CO}_2$  photoreduction with water activated by the UV light irradiation. The result that the CO production rate in the 2nd cycle can be recovered to the similar level in the 1st cycle demonstrates a good cycling capability of the catalyst.

Because the MgAl-LDO may still contain a small amount of carbonate species even after the calcination process, we have conducted another set of experiments to understand the possible interference of carbonate species on the catalyst to the reduction of  $\text{CO}_2$  from the gas phase. Tests were carried out by comparing the photocatalytic activity of 10% MgAl-LDO/ $\text{TiO}_2$  under two gas environments: (1) helium ( $\text{He}$ ) +  $\text{H}_2\text{O}$  vapor and (2)  $\text{CO}_2$  +  $\text{H}_2\text{O}$  vapor, and the results are shown in Fig. 6b. There was no CO production in the  $\text{He}$  +  $\text{H}_2\text{O}$  atmosphere at  $50^\circ\text{C}$ , but when the temperature was increased to  $150^\circ\text{C}$ , CO was produced at a rate of about  $1.0 \mu\text{mol g}^{-1} \text{h}^{-1}$ . This result indicates that carbonates in MgAl-LDOs were stable at low temperatures but were activated at higher temperatures and reduced to CO through photocatalytic reactions. By contrast, when  $\text{CO}_2$  was present, the CO production rate was much higher,  $1.5 \mu\text{mol g}^{-1} \text{h}^{-1}$  at  $50^\circ\text{C}$  and  $4.3 \mu\text{mol g}^{-1} \text{h}^{-1}$  at  $150^\circ\text{C}$ . Comparison of these results suggests that carbonate residues in the MgAl-LDO/ $\text{TiO}_2$  composites did not have significant contribution to the CO production and most of these were derived from gas-phase  $\text{CO}_2$  reduction. To further verify the source of CO production, additional experiments were conducted to measure the photocatalytic activity of  $\text{H}_2\text{Ti}_3\text{O}_7$  and  $\text{TiO}_2$  cuboids in the  $\text{He}/\text{H}_2\text{O}$  atmosphere, and the result is shown in Fig. S7.† No CO production was observed for  $\text{H}_2\text{Ti}_3\text{O}_7$  and  $\text{TiO}_2$  cuboids at either  $50^\circ\text{C}$  or  $150^\circ\text{C}$ . Only 10% MgAl-LDO/ $\text{TiO}_2$  showed some CO production at  $150^\circ\text{C}$ . This result further proved that the small amount of CO produced in the  $\text{He}/\text{H}_2\text{O}$  atmosphere was attributed to carbonate residues in the MgAl-LDO component of the composite and not from carbon contamination of  $\text{TiO}_2$ .

On the other hand, the above interesting finding suggests that if we pre-load carbonates on the composite catalyst by capturing  $\text{CO}_2$  first and then exposing the material under UV light or sunlight, it is possible that we can convert the captured  $\text{CO}_2$  into CO in the second step, and thus we can separate the  $\text{CO}_2$  capture and conversion process. A benefit of doing this is to achieve separation of  $\text{CO}_2$  conversion products (e.g., CO) from the bulk  $\text{CO}_2$ , an approach advantageous to most  $\text{CO}_2$  photoreduction processes reported in the literature where the products are mixed with unreacted  $\text{CO}_2$ . We will conduct further research to investigate this novel idea.

## 4. Conclusions

This work has demonstrated the successful synthesis of novel hybrid materials, MgAl-LDO platelets grafted on  $\text{TiO}_2$  cuboids, with a controlled mass ratio of MgAl-LDO to  $\text{TiO}_2$ . The surface coverage of MgAl-LDO on  $\text{TiO}_2$  and the reaction temperature are two important parameters that influence the activity of  $\text{CO}_2$  photocatalytic reduction to CO. The hybrid MgAl-LDO/ $\text{TiO}_2$  showed a CO production rate five times higher than that of bare  $\text{TiO}_2$  at the optimum 10 wt.% MgAl-LDO loading and at  $150^\circ\text{C}$ . The possible reason for the enhancement is that the grafted MgAl-LDO functions as a  $\text{CO}_2$  adsorbent and its  $\text{CO}_2$  capture ability increases with increasing temperature (below  $200^\circ\text{C}$ ) and that the photoinduced electrons generated on  $\text{TiO}_2$  may migrate to the interfacial sites and promote  $\text{CO}_2$  reduction. At too high a loading of MgAl-LDO when the platelets completely cover the  $\text{TiO}_2$  cuboid surface, the light absorption ability is impaired and the contact between  $\text{TiO}_2$  and  $\text{CO}_2$  is blocked, and thus no improvement in  $\text{CO}_2$  photoreduction is observed. The carbonate residues on the MgAl-LDO/ $\text{TiO}_2$  have a minor contribution to the CO production under photoirradiation, which inspires a new process of sequential  $\text{CO}_2$  capture and photocatalytic conversion to fuels using this novel hybrid material. In this case, the products can be effectively separated from unreacted  $\text{CO}_2$ . This interesting idea will be validated in our future work.

## Acknowledgements

The authors acknowledge the financial support from National Science Foundation (NSF) Early Faculty CAREER Award (CBET-1254709).

## References

- 1 C. Y. Zhao, A. Krall, H. L. Zhao, Q. Y. Zhang and Y. Li, *Int. J. Hydrogen Energy*, 2012, **37**, 9967–9976.
- 2 L. J. Liu, D. T. Pitts, H. L. Zhao, C. Y. Zhao and Y. Li, *Appl. Catal., A*, 2013, **467**, 474–482.
- 3 L. J. Liu, H. L. Zhao, J. M. Andino and Y. Li, *ACS Catal.*, 2012, **2**, 1817–1828.
- 4 Y. Li, W. N. Wang, Z. L. Zhan, M. H. Woo, C. Y. Wu and P. Biswas, *Appl. Catal., B*, 2010, **100**, 386–392.
- 5 Q. Y. Zhang, Y. Li, E. A. Ackerman, M. Gajdardziska-Josifovska and H. L. Li, *Appl. Catal., A*, 2011, **400**, 195–202.
- 6 C. L. Yu, Q. Z. Fan, Y. Xie, J. C. Chen, Q. Shu and J. C. Yu, *J. Hazard. Mater.*, 2012, **237**, 38–45.
- 7 C. Y. Zhao, L. J. Liu, Q. Y. Zhang, J. Wang and Y. Li, *Catal. Sci. Technol.*, 2012, **2**, 2558–2568.
- 8 H. L. Zhao, L. J. Liu, J. M. Andino and Y. Li, *J. Mater. Chem. A*, 2013, **1**, 8209–8216.
- 9 I. H. Tseng, J. C. S. Wu and H. Y. Chou, *J. Catal.*, 2004, **221**, 432–440.
- 10 R. Asahi, T. Morikawa, T. Ohwaki, K. Aoki and Y. Taga, *Science*, 2001, **293**, 269–271.



- 11 Y. Kohno, H. Hayashi, S. Takenaka, T. Tanaka, T. Funabiki and S. Yoshida, *J. Photochem. Photobiol., A*, 1999, **126**, 117–123.
- 12 L. J. Liu, C. Y. Zhao, H. L. Zhao, D. Pitts and Y. Li, *Chem. Commun.*, 2013, **49**, 3664–3666.
- 13 L. Liu, C. Zhao, D. Pitts, H. Zhao and Y. Li, *Catal. Sci. Technol.*, 2014, **2014**, 1539–1546.
- 14 Y. Kohno, H. Ishikawa, T. Tanaka, T. Funabiki and S. Yoshida, *Phys. Chem. Chem. Phys.*, 2001, **3**, 1108–1113.
- 15 Q. Y. Li, L. L. Zong, C. Li and J. J. Yang, *Appl. Surf. Sci.*, 2014, **314**, 458–463.
- 16 S. J. Xie, Y. Wang, Q. H. Zhang, W. Q. Fan, W. P. Deng and Y. Wang, *Chem. Commun.*, 2013, **49**, 2451–2453.
- 17 G. Xiao, R. Singh, A. Chaffee and P. Webley, *Int. J. Greenhouse Gas Control*, 2011, **5**, 634–639.
- 18 A. Chakradhar and U. Burghaus, *Surf. Sci.*, 2013, **616**, 171–177.
- 19 Y. S. Gao, Z. Zhang, J. W. Wu, X. F. Yi, A. M. Zheng, A. Umar, D. O'Hare and Q. Wang, *J. Mater. Chem. A*, 2013, **1**, 12782–12790.
- 20 J. W. Wang, L. A. Stevens, T. C. Drage and J. Wood, *Chem. Eng. Sci.*, 2012, **68**, 424–431.
- 21 M. Dadwhal, T. W. Kim, M. Sahimi and T. T. Tsotsis, *Ind. Eng. Chem. Res.*, 2008, **47**, 6150–6157.
- 22 T. Bujdoso, A. Patzko, Z. Galbacs and I. Dekany, *Appl. Clay Sci.*, 2009, **44**, 75–82.
- 23 K. Teramura, S. Iguchi, Y. Mizuno, T. Shishido and T. Tanaka, *Angew. Chem., Int. Ed.*, 2012, **51**, 8008–8011.
- 24 M. Q. Zhao, Q. Zhang, J. Q. Huang and F. Wei, *Adv. Funct. Mater.*, 2012, **22**, 675–694.
- 25 Y. Kuang, L. N. Zhao, S. A. Zhang, F. Z. Zhang, M. D. Dong and S. L. Xu, *Materials*, 2010, **3**, 5220–5235.
- 26 M. K. R. Reddy, Z. P. Xu, G. Q. Lu and J. C. D. Da Costa, *Ind. Eng. Chem. Res.*, 2006, **45**, 7504–7509.
- 27 M. Leon, E. Diaz, S. Bennici, A. Vega, S. Ordonez and A. Auroux, *Ind. Eng. Chem. Res.*, 2010, **49**, 3663–3671.
- 28 J.-I. Yang and J.-N. Kim, *Korean J. Chem. Eng.*, 2006, **23**, 77–80.
- 29 X. P. Wang, J. J. Yu, J. Cheng, Z. P. Hao and Z. P. Xu, *Environ. Sci. Technol.*, 2008, **42**, 614–618.
- 30 Z. Yang, G. Du, Z. Guo, X. Yu, Z. Chen, T. Guo and H. Liu, *J. Mater. Chem.*, 2011, **21**, 8591–8596.
- 31 Q. Li, J. Zhang, B. Liu, M. Li, S. Yu, L. Wang, Z. Li, D. Liu, Y. Hou, Y. Zou, B. Zou, T. Cui and G. Zou, *Cryst. Growth Des.*, 2008, **8**, 1812–1814.
- 32 Q. Li, J. Zhang, B. Liu, M. Li, R. Liu, X. Li, H. Ma, S. Yu, L. Wang, Y. Zou, Z. Li, B. Zou, T. Cui and G. Zou, *Inorg. Chem.*, 2008, **47**, 9870–9873.
- 33 J. Wang, D. D. Li, X. A. Yu, M. L. Zhang and X. Y. Jing, *Colloid Polym. Sci.*, 2010, **288**, 1411–1418.
- 34 N. C. S. Selvam, R. T. Kumar, L. J. Kennedy and J. J. Vijaya, *J. Alloys Compd.*, 2011, **509**, 9809–9815.
- 35 Y. S. Zhao, J. G. Li, F. Fang, N. K. Chu, H. Ma and X. J. Yang, *Dalton Trans.*, 2012, **41**, 12175–12184.
- 36 Š. Paušová, J. Krýsa, J. Jirkovský, G. Mailhot and V. Prevot, *Environ. Sci. Pollut. Res.*, 2012, **19**, 3709–3718.

